Climatologies of blocking highs detected by a unified Eddy-ABS approach

Ping Liu[1]

Abstract

Typical blocking indices in longitude or both longitude and latitude are compared to demonstrate: (1) the central blocking latitude (CBL) should be any of 40–80° N; (2) reversals of meridional gradients in absolute fields (ABS) about specified CBLs or in combination with time anomalies exceeding a threshold missed blocking patterns or misidentified non-blocking structures. Blocking highs are identified by a new Eddy-ABS index. A large-scale high is represented by a local maximum of zonal eddy anomalies, its immediately surrounding points and subsequent contiguous grids with decreasing anomalies but exceeding the 75th percentile. A high with any ABS reversal is an instantaneous blocking (IB). Maximum overlapping IBs become quasi-stationary when moving less than 10° longitudes per day. Four and more quasi-stationary IBs form a blocking event (BE). This unified index has identified IBs and BEs at vertical levels in the Northern (NH) and Southern Hemispheres (SH) during different seasons. In the NH, BEs exhibit strong seasonality, geographical preference and quasi-barotropicity. The lifetime, maximum intensity, impact area, and moving speed have a log-linear, log-normal, log-normal, and normal distribution, respectively. These features occur similarly in the SH, except for very small occurrences at 200 hPa in JJA and a normal distribution for the maximum intensity. Properties other than the moving speed significantly correlate with the maximum intensity in both hemispheres. The missing and misidentification issues are reasonably well resolved by this new index.

1 Introduction

Atmospheric blocks are large-scale flow patterns blocking migratory cyclones and storm tracks in mid-high latitudes (Rex 1950; Tibaldi and Molteni 1990, TM1990 hereafter; Pelly and Hoskins 2003; Woollings et al. 2018) to induce high-impact weather events and disastrous climate in all seasons (Carrera et al. 2004; Pfahl and Wernli 2012; Park and Ahn 2014; Yamada et al. 2016; Brunner et al. 2017; Rodrigues and Woollings 2017). There are five canonical instantaneous blocking (IB) patterns on 500-hPa geopotential height (Z500) charts in the NH (Woollings et al. 2018): an omega shape blocking (Fig. 1a), a cutoff high (Fig. 1b), a Rex dipole (Fig. 1c), an anticyclonic wave breaking with the high extending northeastward (Fig. 1d), and a cyclonic wave

breaking with the high extending northwestward (Fig. 1e; also a Rex dipole in this case). These blocking patterns generally share three characteristics: obstruction of the usual mid-latitude westerly flow with a substantial reduction or a reversal to easterly, quasi-stationarity in space (Fig. 1a, b), and persistence for days to even weeks. The quasi-barotropicity corresponds to patterns at Z200 sometimes similar to those at Z500 (Fig. 1a2–e2; Pelly and Hoskins 2003). Similar quasi-barotropic structures occur at Z850 and will be demonstrated in Sect. 6. It is noteworthy that each of the five IBs has a high component that is well collocated with the 75th percentile (gray shading) and less well with the 90th (blue dots) of zonal eddy anomalies (see definitions in Sect. 2).

Because blocking characteristics vary substantially in time and space, the detection of IBs, their subsequent quasi-stationarity and persistence into BEs has been a challenge and motivated many researchers to develop different indices during past decades (reviews by Diao et al. 2006; Barriopedro et al. 2010; Woollings et al. 2018; Table 2 in "Appendix" for a brief comparison). In particular, the TM1990, a widely

✉ Ping Liu
ping.liu@stonybrook.edu

1   Endeavor Hall 199, School of Marine and Atmospheric Sciences, Stony Brook University, Stony Brook, NY 11794-5000, USA
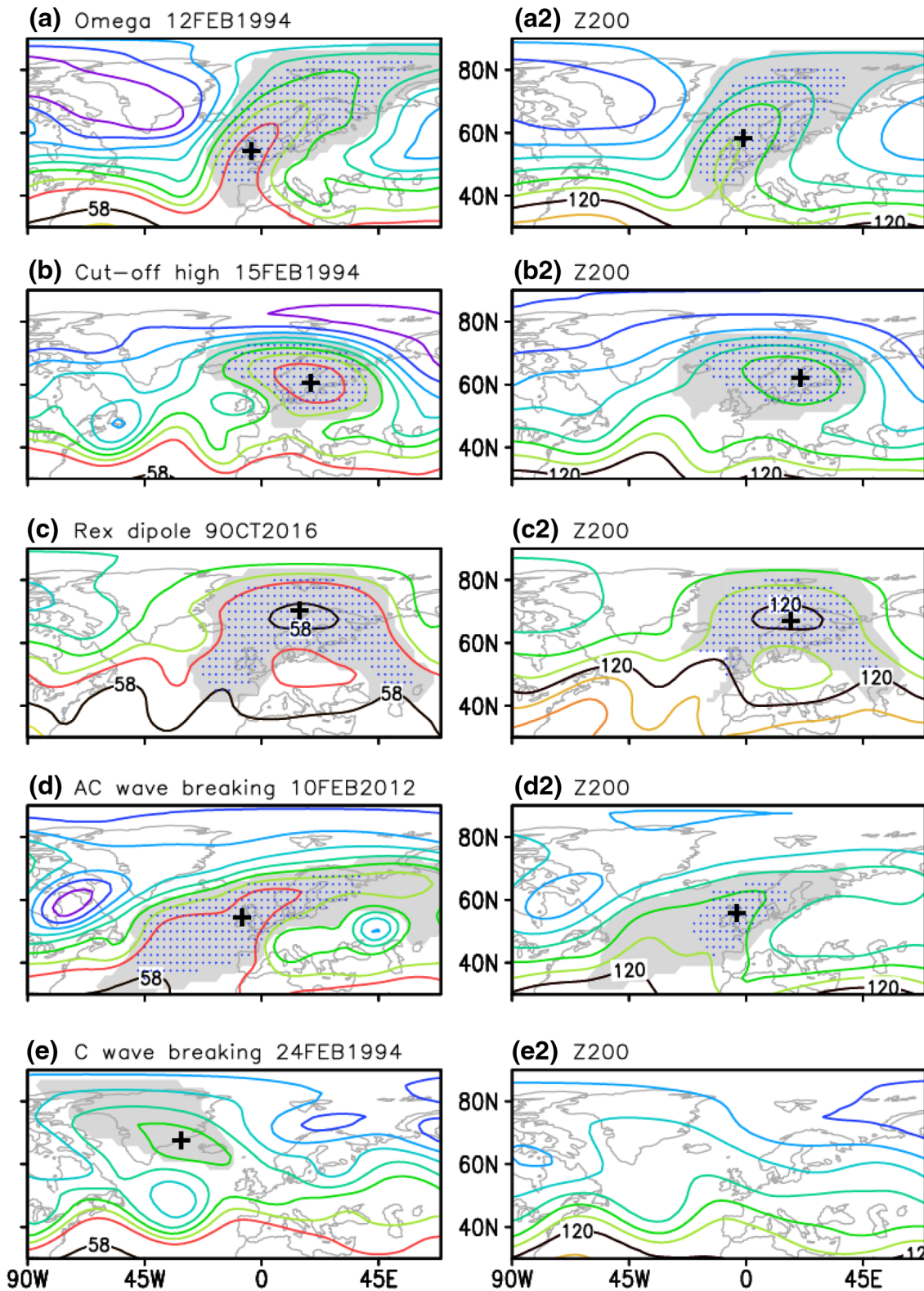
Fig. 1 Five canonical IB patterns at Z500 (left) and Z200 (right). The contours labeled 58 and 120 represent 5800 and 12,000 geopotential meters (GPM), and the intervals are 100 and 200 GPM. The plus sign marks the approximate center of the pattern. Gray shading represents a blocking high where zonal eddy anomalies are greater than the 75th (blue dots for the 90th) percentile decreasing from the local maximum and correspond to at least one reversal of meridional gradients of Z500 or Z200 on its member grids between 40° N and 80° N

Fig. 2 CBLs represented by the maximum climatological synoptic variance of 5-day hig-pass filtered eddy kinetic energy (EKE) at 300 hPa (EKE300; black) and 500 hPa (EKE500; red), and Z500 (blue) on each 4° longitude in the NH during DJF (**a**) and JJA (**b**). Green dashed lines are 60° N and 52° N
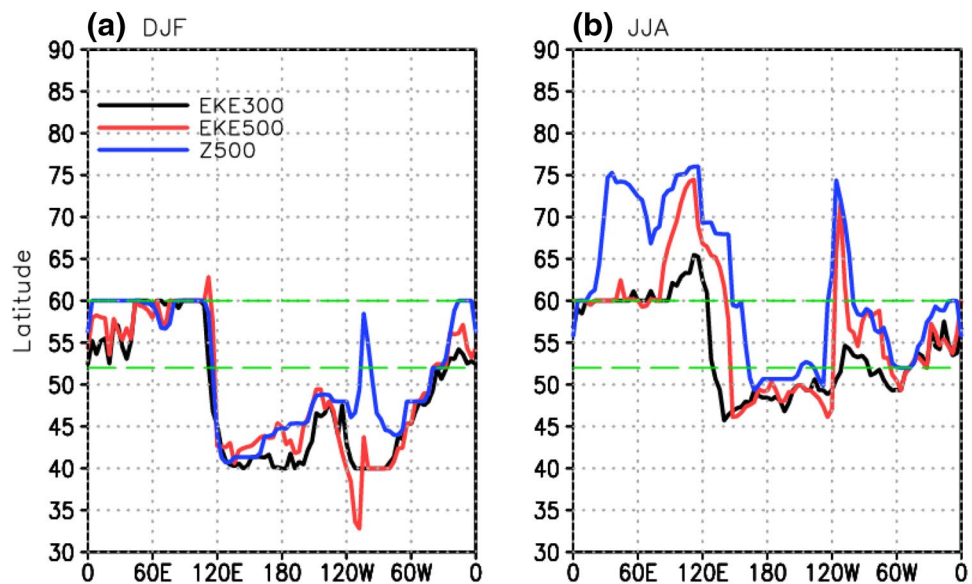
adopted 1-D index as a slight modification of Lejenäs and Økland (1983), emphasized an established reversal of meridional gradients of Z500 in mid-high latitudes. The approach specified 60° N as the CBL, about which the gradients with 80° N in the north (GHGN) and with 40° N in the south (GHGS) were compared for possible reversals as IBs. The sector in the Pacific or Atlantic-Europe was blocked with at least three adjacent IBs being present. A BE was characterized by successive sector blockings for at least 4 days. Among the specifications, the single CBL fixed at 60° N to represent the location of jet streams for all cases is particularly questionable. Pelly and Hoskins (2003) proposed that the CBL should at least vary in longitude and follow the latitudes where the maximum climatological variances of synoptic eddy kinetic energy at 300 hPa (EKE300) were located, because these latitudes better depicted the seasonal variations of jet streams. The TM1990 incorporated with the EKE300 CBLs (1D-ABS in short) detected quite different blocking occurrences with particularly less instances in the Pacific and notably more near 120° W (Fig. 2 and discussions below). Which systems were missed or misidentified by the 1D-ABS remains outstanding, however.

Later 2-D indices were designed to detect blocks in both longitude and latitude. The first group of 2-D approaches expanded the TM1990 to the latitude direction. Scherrer et al. (2006) modified the TM1990 by specifying the CBLs at any latitude between 35° N and 75° N and a 15° distance was used to compute the GHGN and GHGS. A grid was blocked if the original thresholds were satisfied consecutively for 5 days. The condition restricted on each grid resulted in smaller blocking occurrences than those detected by the TM1990 and its variants (D'Andrea et al. 1998; Doblas-Reyes et al. 2002). Furthermore, that 2-D index did not consider the spatial extension of blocks. Davini et al.

(2012) introduced a spatial persistence constraint (2D-ABS or the ABS in Woollings et al. 2018) by defining large-scale blocking (LSB) events as IBs extending for at least 15° longitudes and a BE as LSBs within a box of 5° latitudes by 5° longitudes centered on the grid point for at least 5 days. They added a condition that a second GHGS2 to the south of GHGS must be smaller than −5 GPM/° to avoid cut-off lows and subtropical features. The resultant occurrences of IBs and BEs were quite different from those in the original TM1990 (more details below). Which systems were missed or misidentified to cause the differences remains outstanding as well.

The other group of 2-D indices focused on the anticyclonic area of a blocking by searching anomalous fields as departures from the climatological mean exceeding a given threshold (Dole and Gordon 1983; Dole 1986; Sausen et al. 1995; Schwierz et al. 2004; Barriopedro et al. 2010; Dunn-Sigouin et al. 2013). Woollings et al. (2018) updated and named the purely anomaly index as ANO. It detected an IB as daily Z500 anomalies above the 90th percentile of distributions in 50–80° N and covering at least 2×10^6 km^2. Quasi-stationarity and persistence were ensured by imposing a minimum percentage (50%) of spatial overlap successively for at least 5 days. Two issues remain in the ANO, however: (1) whether the 90th percentile can correspond to weak highs collocated with a climatological trough, and (2) how the 50% overlap is translated into a moving speed of IBs to meet the quasi-stationary requirement for BEs.

Barriopedro et al. (2010) reconciled the TM1990 and ANO as a hybrid approach. The index first determined the reversals of meridional gradients in Z500 for IBs by computing 15°-latitude averaged height to the north and south of the CBL. The CBL followed the maximum of synoptic variance at Z500, which will be shown close to that of the EKE300.

Nevertheless, each CBL still corresponded to fixed latitude at each longitude, different from any latitude as a CBL in Scherrer et al. (2006). The hybrid index then extended the zonal detection by identifying contiguous anomalies above 1 STD and tracked the IBs with 50% overlapping and persistence of 4 days as BEs.

Dunn-Sigouin et al. (2013) designed a similar hybrid index by switching the order of computing the ABS and ANO. They first considered the ANO above 1.5 STD as candidates, and then tracked them for blocking anomalies by imposing three critical thresholds: a spatial scale of 2.5×10^6 km^2, 50% overlapped area in 2 days, and persistence for 5 consecutive days. The tracked blocking anomalies were then tested for an ABS reversal for BEs. The reversal was determined as negative Z gradient to the south of the maximum anomaly. Woollings et al. (2018) revised the hybrid indices of Barriopedro et al. (2010) and Dunn-Sigouin et al. (2013) as the MIX by (1) first using the 90th percentile to replace the 1 and 1.5 STD (~78th percentile) to determine blocking anomalies, and (2) considering the CBL as the latitude of climatological maximum synoptic variance of Z500. Whether specified CBLs in the ABS and MIX caused significantly different blocking climatologies is an open question.

In additional to the aforementioned issues, two more remain outstanding in blocking detection. One is that blocks at Z500 in the SH have not been systematically detected to compare with those in the NH, although some authors implied that their approach should be similarly applied. The other is that quasi-barotropicity is known to characterize blocking, while a direct comparison of blocks between Z500 and Z200 and even Z850 lacks to demonstrate the unique vertical structure. Meanwhile the diversity of blocking indices and definitions make it difficult to compare blocking diagnostics. The issues and limitations demand a unified index to explain the differences and apply to the lower, middle and upper troposphere in both the NH and SH during different seasons.

Liu et al. (2018) demonstrated that a high or ridge of Z500 was well represented by positive zonal eddy anomalies Z^* in both magnitude and location, since removing the zonal means did not change the zonal gradients of Z500 or meridional winds. They specified the threshold of 100 GPM in Z^* for a ridge or high in any case. This threshold should be allowed to change with time, such as by using high percentiles of Z^* in 40–80° N for each month. As an example, the gray-shading for Z^* above the 75th percentile in February and October are reasonably well collocated with the five canonical blocking patterns at Z500 and Z200 (Fig. 1). Combining Z^* above a percentile and the reversals in meridional gradients of Z appears promising to form the preferred 2-D blocking index.

We hypothesize that the specified CBL at each longitude either fixed at 60° N or following the maximum synoptic variance is the primary cause of the significantly different blocking climatologies detected by existing indices. Instead, any latitude inside the interval of (40°, 80°) should be examined for a possible reversal to reasonably reflect the daily variations of jet streams and blocking. This hypothesis will be examined by comparing the several indices discussed above, with a focus on missed blocking patterns and misidentified non-blocking structures. Section 2 introduces the data and methods. Sections 3 and 4 analyze and compare five typical blocking indices with different CBL configurations to understand the different IB and BE climatologies caused by specified CBLs and time anomalies. Section 5 describes the new 2-D Eddy-ABS index combining zonal eddy anomalies and the CBL at any latitude. Section 6 presents the climatologies of blocking highs in the NH and SH at different vertical levels during DJF and JJA. The climatologies of occurrence frequencies, lifetime, intensity, longitudinal width, longitude-latitude area, and moving speeds of tracked blocking highs are derived, and some are compared with those detected by the typical indices to understand the known geographical preference, seasonality and quasi-barotropicity of blocking, and to disclose possible linear relationships among these features, in particular in reference to the maximum intensity of BEs. Summary and discussions are given in Sect. 7.

2 Data and methodology

2.1 Data

The daily data are derived from the NCEP-NCAR Reanalysis project (Kalnay et al. 1996), including geopotential heights at 850, 500, and 200 hPa, zonal and meridional winds at 300 and 500 hPa for computing the eddy kinetic energy. All fields cover 1 January 1979–28 February 2019 at a resolution of 2.5° × 2.5° longitudes by latitudes. A bilinear algorithm interpolates the data to 4° × 4° for comparing the TM1990 index and its variants. This data set was used for detecting blocking in previous studies (Renwick 2005; Barriopedro et al. 2006, 2010; Diao et al. 2006; Dunn-Sigouin et al. 2013; Davini et al. 2014; Colucci and Kelleher 2015; Sousa et al. 2017).

The Z500 from the ERA5 Reanalysis (C3S; 2017) at resolutions up to 0.25° × 0.25° are derived to examine the sensitivity of detected blocks to data source and resolution. In particular, the resolutions of 0.25° × 0.25°, 0.5° × 0.5°, 1° × 1°, 2° × 2° and 4° × 4° are based to compare the TM1990 and resultant BE climatologies with the NCEP-NCAR reanalysis.

2.2 Zonal eddy anomalies

Daily zonal eddy anomalies Z^* are derived by simply removing the zonal means from Z. Liu et al. (2018) demonstrated how Z^* at 500 hPa well represented a ridge or high in both magnitude and location in comparison with deviated time anomalies Z'. That is because climatological eddy components $\bar{Z}^*$ are retained in Z^* but eliminated in Z'. The $\bar{Z}^*$ include stationary perturbations induced by large mountains in the NH, which is an essential factor to blocking formation. After $\bar{Z}^*$ is removed, a positive Z' may correspond to a weak ridge or high in Z where a climatological trough is located. This caveat of Z' is demonstrated below to cause the MIX to detect many saddle structures in JJA as blocking in the west of Greenland where a climatological trough is located.

2.3 Percentiles distributions of zonal eddy anomalies

Rather than a specified positive value (e.g., 100 GPM in Liu et al. 2018) for determining a blocking-high candidate, the thresholds in Z^* percentile are derived from 3-month centered distributions. The values in 40°–80° inclusive are sorted and the 50th–90th percentiles are determined. These percentiles are slightly different from those of 50°–80° in the NH and more reasonable than the narrower range in the SH (not shown). More tests with different percentiles in determining blocking highs are discussed below. The distributions and percentiles of Z' are similarly derived, while those in 50–80° N are used to define the ANO and MIX indices for comparison.

2.4 Synoptic-scale variance

The daily time series of EKE300 and EKE500 are computed from anomalous horizontal winds. The same series for Z500 are also derived. These data sets are then filtered with a 5-day high-pass filter. To compute the variance, a 90-day filtered time series is selected in a way that it centers on the 15th day of a month and extends half backward and half forward with adjustments on both ends of the data. The variances of the time series in the nearest 25 years are averaged as the climatological variance. The latitudes with the maximum climatological variances of EKE300, EKE500 or Z500 on a longitude are recorded as the CBL for that month in the comparisons below.

3 Specified CBLs cause distinct blocking occurrences in the TM1990

3.1 Specified CBLs

Several CBLs were adopted in most existing blocking indices, and they are reproduced in Fig. 2 for comparison. The

60° N was used in the TM1990 and several variants, while the latitudes of maximum climatological synoptic variance of EKE300 were adopted by Pelly and Hoskins (2003; black in Fig. 2). Maximum EKE300 latitudes vary notably in DJF and JJA with an overall northward shift. This variability was believed to better consider the seasonality of blocking occurrences. The maximum climatological synoptic variance of EKE500 (red in Fig. 2) follows the EKE300 well in DJF, while it drifts much more poleward during JJA. The latitudes of maximum climatological synoptic variance of Z500 were the CBLs in the MIX index of Woollings et al. (2018; blue in Fig. 2). This variance generally agrees with the EKE500 and EKE300 in DJF, and with the EKE500 in JJA, except for some differences in several longitudes. Also illustrated in Fig. 2 is the 52° N, near the average of other CBLs in DJF and slightly south of the EKE300 in JJA. These CBLs are next shown to lead to notably different blocking occurrence climatologies detected by the TM1990.

3.2 Distinct blocking occurrences with different CBLs

The TM1990 is based to demonstrate how differently specified CBLs lead to different occurrence climatologies of IBs and BEs at Z500 in the NH during DJF and JJA seasons. Other original settings are retained; in particular, the data are bi-linearly interpolated to 4°×4° longitude by latitude. The results are nearly identical at the several resolutions up to 0.25°×0.25° in the latest ERA5 Reanalysis (C3S 2017; not shown).

Five CBLs, i.e., 60° N, 52° N, EKE300, EKE500 and Z500, have detected climatological IB occurrence frequencies with somewhat similar seasonality and geographical preferences (Fig. 3). For example, in DJF the frequencies have a primary peak in the Atlantic-Europe sector and a secondary peak in the Pacific-North America sector. In JJA the two winter maxima drop substantially such that there are about six peaks at 10–15%. These features have been disclosed before (e.g., Pelly and Hoskins 2003).

There are notable differences in the IB frequencies among the CBL configurations. In DJF the primary peak of occurrence is nearly 29% at about 10° E for the 52° N CBL as the largest (black-dashed in Fig. 3a), while it is only slightly above 20% for the CBLs fixed at 60° N (black-solid) and the maximum synoptic variance of Z500 (blue). Also notable is that the IB frequencies have a secondary peak about 15% in the central-eastern Pacific for the 60° N CBL. In all other CBLs the secondary peak shifts eastward to around 120° W and the occurrences drop dramatically to less than 5% in the central Pacific. In JJA (Fig. 3b), the 52° N CBL detects most IB occurrences of 22% near 30° E, and the Z500 CBL detects about 10%, only a half and indicating a notable difference.
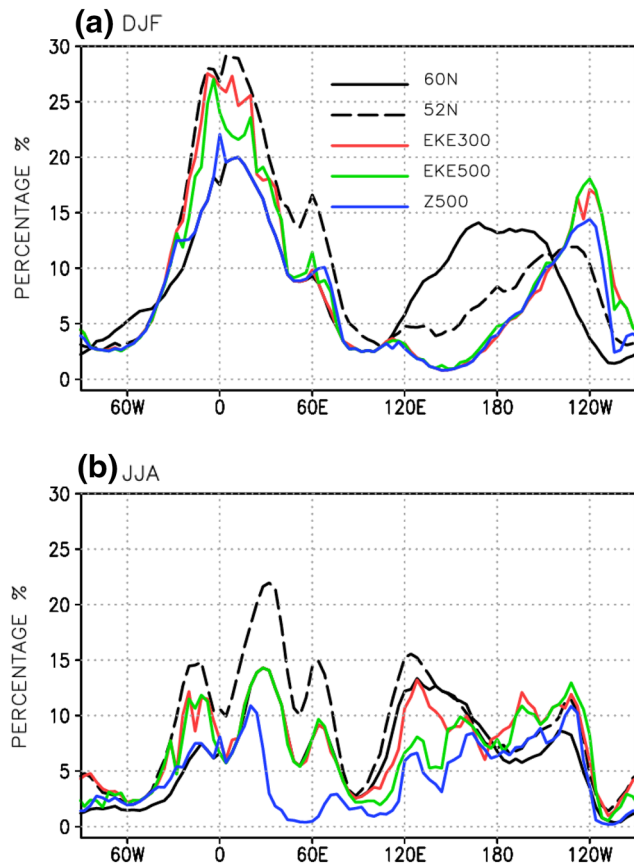
Fig. 3 Climatological IB occurrence frequencies detected by the TM1990 index with different CBLs in DJF (**a**) and JJA (**b**)

Some differences in fact correspond to blocking patterns missed by the CBLs of 52° N, EKE300, EKE500 and Z500. This is demonstrated by a composite of Z500 for 312 IBs at 160° E in DJF (cf. Fig. 3a) detected by the 60° N CBL but not by the 52° N CBL (Fig. 4). Clearly the composite has a Rex dipole tilted slightly southwest-northeast; the center of the high is located at 65° N and the center of the low at 49° N. The 52° N CBL is too close to the low center to detect the reversals of meridional gradients occurring in the north around 60° N, resulting in the misses. The synoptic-variance CBLs are even farther south (about 42° N in Fig. 2) along 160° E such that these CBLs have barely detected the IB cases either (not shown). It is noteworthy that the composited high is well collocated with Z^* above the 75th percentile (gray shading in Fig. 4), indicating that those highs can potentially be identified when Z^* are combined with the reversal of meridional gradients of Z at any grid in the high. The 90th percentiles of both Z^* and Z', however, exceed the strength of the highs, such that the ANO and MIX of Woollings et al. (2018) can hardly detect these relatively weak highs (not shown). More composites of Z500 for the IBs at 0° E and 120° W missed by the CBL fixed at 60° N but captured by other CBLs are typical blocking patterns as well. In particular at 120° W, 570 IBs mostly in omega type (not shown) are missed by the 60° N CBL compared to the EKE500 CBL that is much more northward. These composites indicate that fixed CBLs close to the low tend to miss the gradient reversals and IBs, although each missed case may have a pattern slightly different from the composites.

Fig. 4 Composite of Z500 for the IBs at 160° E during DJF 1979–2018 detected by the TM1990 with the CBL at 60° N but not with the CBL at 52° N. There are 312 IBs in total. Gray shading is zonal eddy anomalies greater than the 75th percentile
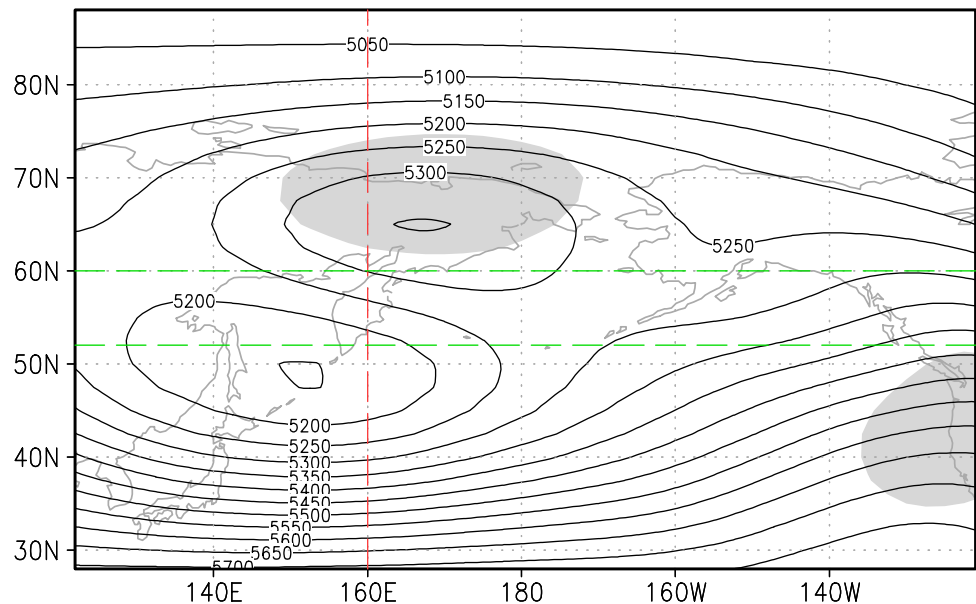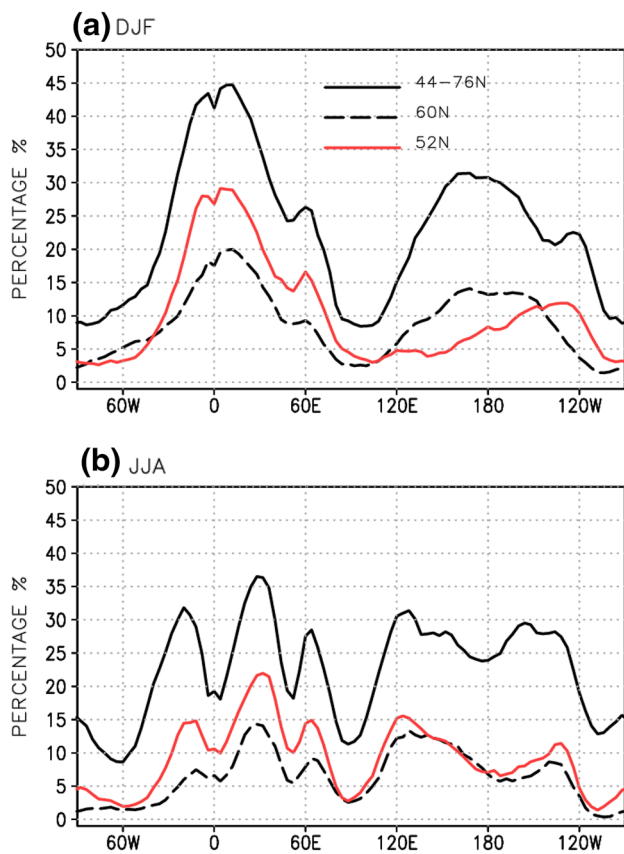
Fig. 5 Same as Fig. 3 but with the CBLs at 60° N (black-dashed), 52° N (red), and any latitude between 44°–76° N inclusive (black-solid)

Motivated by Scherrer et al. (2006) who considered any latitude as the CBL, we have expanded the TM1990 to also consider the CBL anywhere between 44° N and 76° N inclusive. The identified IB frequencies are compared with those by fixed CBLs at 60° N and 52° N (Fig. 5). Not surprisingly the CBL at any latitude has detected notably more IB occurrences everywhere in the NH. For example in DJF (Fig. 5a), the primary peak near 10° E becomes 45% (black-solid), about 1.5 times of that in the 52° N CBL (red) and more than double to that in the 60° N CBL (black dashed), and the secondary peak becomes 32% at 160° E, about double to that in the 60° N CBL (black-dashed) and four times of that in the 52° N CBL (red). Specifically at 160° E, there are 1042 IBs newly detected. The composite of Z500 for these IBs is also a slightly titled Rex dipole, while the high is located further northward to about 70° N (not shown). These highs are reasonably well collocated with Z^* above the 75th percentile as well (not shown). Nevertheless the 1042 IBs may include less-typical blocks as shown in Fig. 9 below. In JJA (Fig. 5b), the CBL at any latitude detected notably more IBs than both the 52° N and 60° N CBLs. The primary peak drops to 36% and shifts eastward to 30° E, indicating

strong seasonality of IB occurrences detected by the CBLs at any of 44–76° N.

The CBL at any latitude also helps detect omega-type IBs, which is demonstrated by the case on 12 February 1994 (cf. Fig. 1a). Each detected IB is represented by blue dots in Fig. 6. The EKE300 and 52° N CBLs have detected only 3 longitudes inside the omega IB as blocked (Fig. 6a, e); the CBLs of 60° N and Z500 synoptic variance have 5 (Fig. 6c, d); the EKE500 CBL has 6 (Fig. 6b); and the CBL at any of 44°–76° N has 14 longitudes (Fig. 6f), covering most of the IB. It is noteworthy that many grids inside and nearby the high component are either missed or misidentified by the CBL at any latitude too, while they are reasonably well collocated with and differentiated by Z^* above the 75th percentile (gray shading in Fig. 6).

Corresponding to the IB climatologies, the BEs are detected notably more by the CBL at any latitude than all other CBL configurations in DJF and JJA seasons, as shown by the bar charts in Fig. 7. The BEs occurred 58% in DJF over the Atlantic-Europe sector by the CBL at any latitude (blue bars). This value is far larger than the frequencies by other CBLs. Similarly notable difference also occurs in the Pacific Sector (green bars). The contrasting IBs and BEs in this section indicate that the CBL should be tested at any latitude in 44–76° N in a blocking index.

4 Misidentifications in the 2-D ABS and MIX

The three 2-D indices ABS, ANO and MIX of Woollings et al. (2018) produced notably different blocking climatologies in the NH as well. The differences are reproduced and shown by a comparison of the maximum occurrence at each longitude in Fig. 8. Also compared (black) is the BE climatology by the 1-D ABS using the EKE300 CBL and relevant definitions (Pelly and Hoskins 2003). The three 2-D indices detected overall more BEs than the 1-D ABS, especially in JJA (Fig. 8b). However, the 2-D indices appear to have notably reduced the geographical preference and seasonality of BE occurrences. In DJF the ANO and MIX have detected two relatively larger occurrences near the date line and 0° E, and the difference between the two is much less dramatic than that by the 1-D ABS (black in Fig. 8a), indicating somewhat reduction in the geographical preference. In JJA the ANO and MIX have detected nearly identical occurrences except for a smaller value in the MIX over the Atlantic-Europe, and the distribution is overall flat with less noticeable peaks in the NH, which contrasts the substantially reduced BE occurrence in the 1-D ABS. Whether the additional occurrences correspond to misidentifications in the 2-D indices or misses in the 1-D ABS has not been investigated and it will be examined below.

In particular, the 2-D ABS (red in Fig. 8) has detected notably more BEs at 160° E than the 1-D ABS (black in
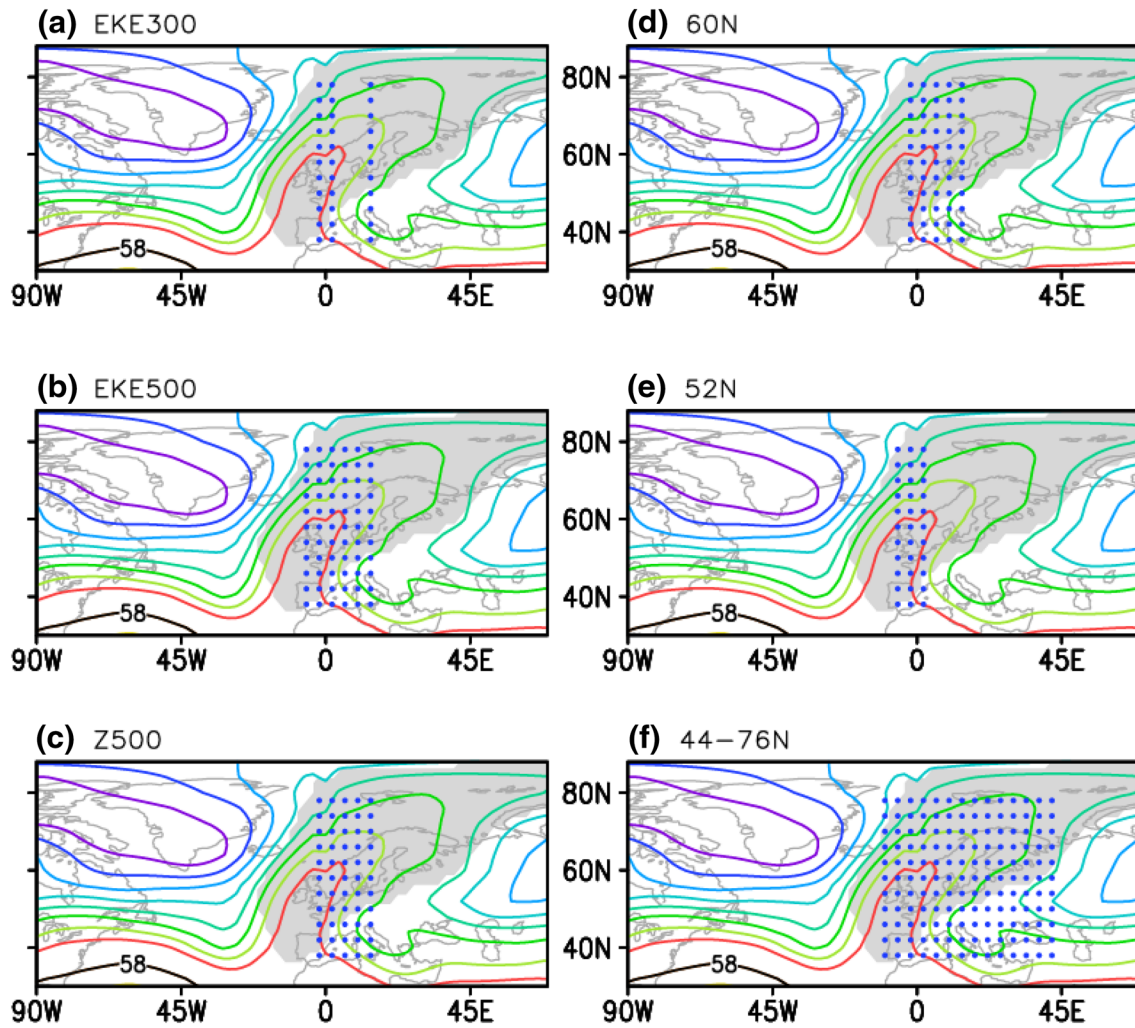
Fig. 6 The omega blocking at Z500 on Feb 12, 1994 detected by TM1990 with different CBLs (blue dots). Gray shading denotes zonal eddy anomalies above the 75th percentile

Fig. 8) in both DJF and JJA. In addition to the contributions from different CBLs discussed in Sect. 3, misidentifications in the 2-D ABS during DJF and in the MIX during JJA are demonstrated by two composites. The first composite corresponds to the peak occurrence of 11% near 160° E in DJF of the 2-D ABS and maximum BE frequencies centered at 160° E, 65° N (shading and blue box in Fig. 9a). The composited Z500 for all these BEs (contours in Fig. 9a) includes a primary cutoff low in the south with a center near 150° E, 50° N and a weak ridge in the north. Although such a pattern meets the blocking requirements in the 2-D ABS, the very weak ridge in the north and very strong westerly in the south represented by large meridional pressure gradients indicate that the jet streams have a major shift to the south by the cutoff low with a marginal split in the north of the low. These marginal patterns would not be identified as IBs or BEs if a blocking high with Z^* above the 75th percentile is required.

The second composite selects the BEs in JJA detected by the MIX near 60° W, 70° N where the occurrence frequency

is about 7% (yellow shading in Fig. 9b; also in Fig. 2 of Woollings et al. 2018). The composited Z500 (contours) indicates a saddle pattern with a low–high structure in the northwest-southeast direction and a low–high dipole in the east–west. These saddle patterns are detected as BEs because the above 90th-percentile Z' are located at the climatological trough in the west of Greenland, as shown by the negative $\bar{Z}^*$ (green-dashed). The Z' with a lower percentile such as the 1.5 STD (~78th) in Dunn-Sigouin et al. (2013) include the patterns as well (not shown). Such a saddle pattern should not be included in IBs, although it meets all the requirements defined in the MIX. The two composites in Fig. 9 indicate that the differences in blocking climatologies detected by 2-D blocking indices are largely caused by misidentifications. These methodological biases need to be corrected systematically. The composites also indicate that a combination of Z^* above the 75th percentile with a reversal of meridional gradients of Z at any grid within the high can
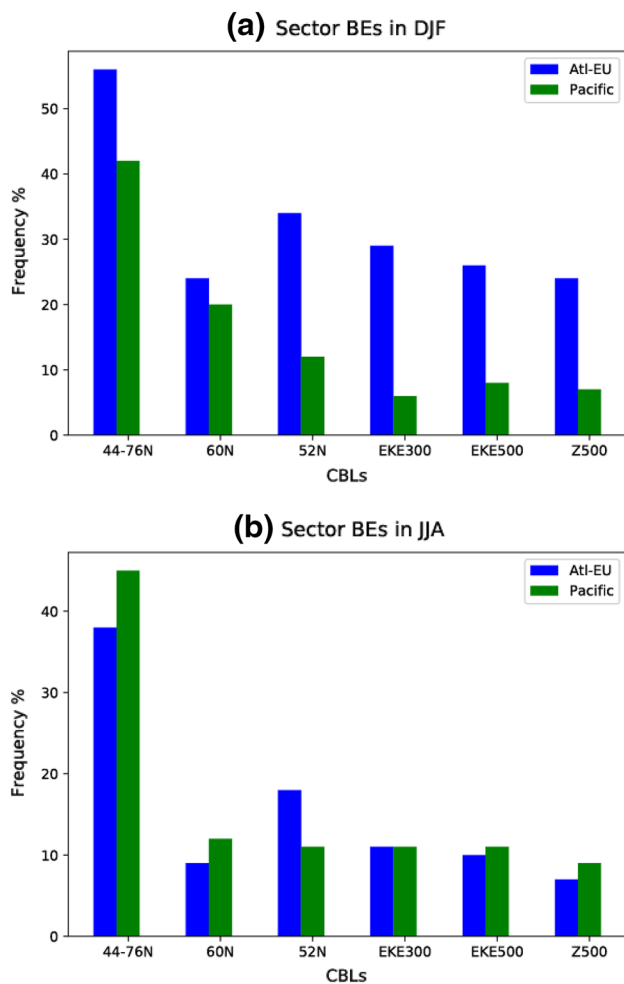
Fig. 7 BE occurrence frequencies in the Atlantic-Europe (blue) and Pacific (green) sectors in DJF (**a**) and JJA (**b**) detected by the TM1990 with different CBLs

Fig. 8 BE occurrence frequencies in DJF (**a**) and JJA (**b**) detected by 1D-ABS (black), 2D-ABS (red), 2D-ANO (green) and 2D-MIX (blue). The values for the 2-D indices are the maximum on each longitude

reasonably resolve the misidentifications. This combined index is described next.

5 A new 2-D Eddy-ABS index for blocking highs

The new index detects four features of IBs and BEs: a high component, a reversal of Z gradients against a CBL inside the high, quasi-stationarity and persistence. The CBL at any latitude between $42.5°$ and $77.5°$ is the first condition of the new index. Other features are ensured by proper thresholds selected below. The selection procedure is unified and applicable to different vertical levels in the NH and SH during different seasons, and the number of parameters is kept at a minimum to reduce the sensitivity, a recommendation by Woollings et al. (2018) in developing a new blocking index.
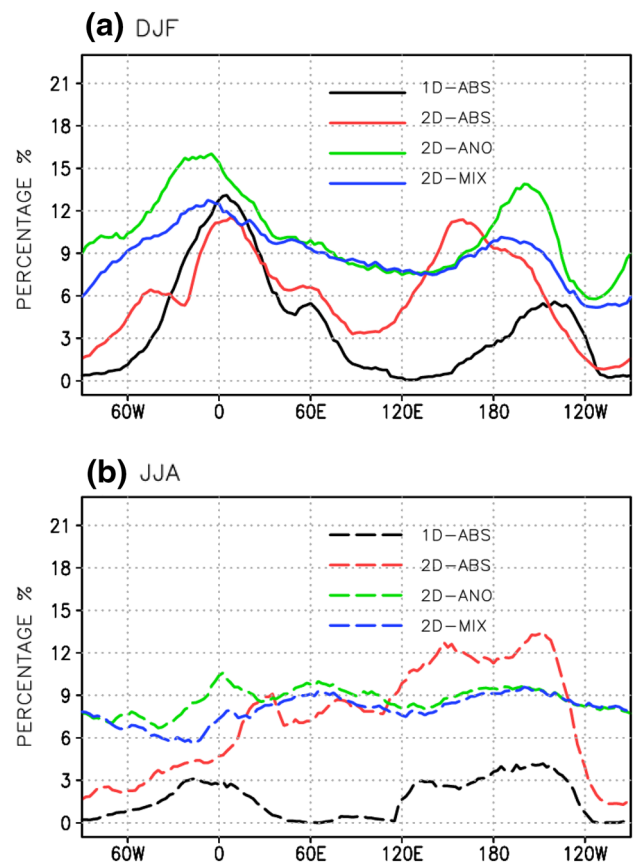
5.1 Identification of the highs

Any positive Z^* is above the zonal mean and represents a ridge or closed high by definition, while an upper percentile of Z^* in $40°$–$80°$ latitude helps to exclude marginal highs. Figure 10 elucidates Z^* percentiles at the 50th, 60th, 70th, 75th, 80th, and 90th. The values are notably higher in cool seasons than in warm ones in the NH and SH. In the NH, the 90th percentile in January reaches a maximum of 120 GPM at Z850[1] (Fig. 10a), 200 GPM at Z500 (Fig. 10b) and 260 GPM at Z200 (Fig. 10c), while the corresponding value in July decreases to a minimum of 75, 110 and 150 GPM, respectively. Similar seasonality also occurs in the SH (Fig. 10d–f), although the differences are smaller. Among these percentiles, the 75th (green) at Z500 in DJF is nearly 100 GPM in the NH, close to the single threshold of 100 GPM for detecting persistent ridges and closed highs in

---

[1] Select grids at Z850 have climatological surface pressures not smaller than 850 hPa.

Fig. 9 BE occurrence frequencies (color shading) in DJF detected by the 2-D ABS (**a**) and in JJA by the MIX (**b**). Black contours are Z500 composites for the BEs occurring inside the blue rectangle, and green-dashed contours (interval of 10 GPM) are negative zonal eddy anomalies of long-term-mean Z500 in JJA representing climatological troughs or lows
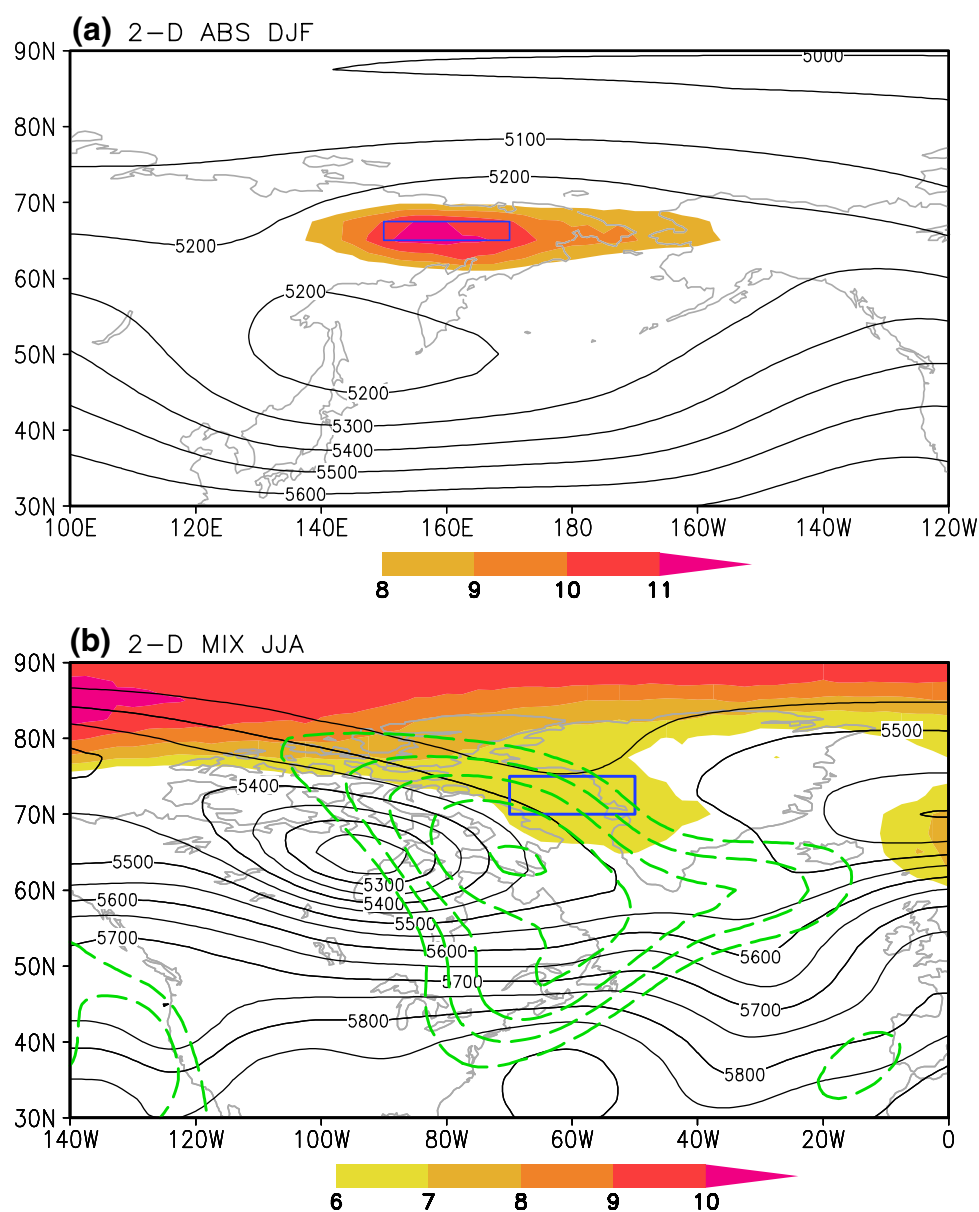
Liu et al. (2018). This percentile has been shown to represent the IBs more properly than the 90th at both Z500 and Z200 (cf. gray shading Fig. 1). Percentiles lower than the 75th include more weak ridges and subtropical highs, and the 80th excludes many relatively strong ridges (not shown). The 75th percentile of Z^* is then selected as the second condition of the new unified blocking index.

A recursive maximum-searching procedure separates adjacent grids with Z^* above the 75th percentile that form more than one high (cf. Fig. 1). A global mask map at the 2.5° × 2.5° resolution is first initialized to zero for updating grid status. The global maximum of Z^* is selected as the first center. This grid and its immediate eight surrounding grids form a core. The core is expanded to contiguous grids with Z^* values in 95–100% of the center to absorb nearby

secondary maxima. The expanded core is further stretched to contiguous grids with Z^* decreasing away. After the expansion, a tail is cut short by retaining only one instance where a single point is next to an inner 2-point row (latitude) or column (longitude). Grids in a hole surrounded by select ones are also included in the high. All select grids are then marked with number one on the mask as the first high. The second high starts from the global maximum Z^* on the rest grids and 0 on the mask map. Similarly, its neighboring and contiguous points are selected and expanded with the tail being cut short and any hole being filled. These select grids are marked with number 2 on the mask map. Subsequent maxima are tested and repeated until all grids are examined on each day. A maximum not forming a core is temporarily marked as 0.5 and eventually reset back to 0 on
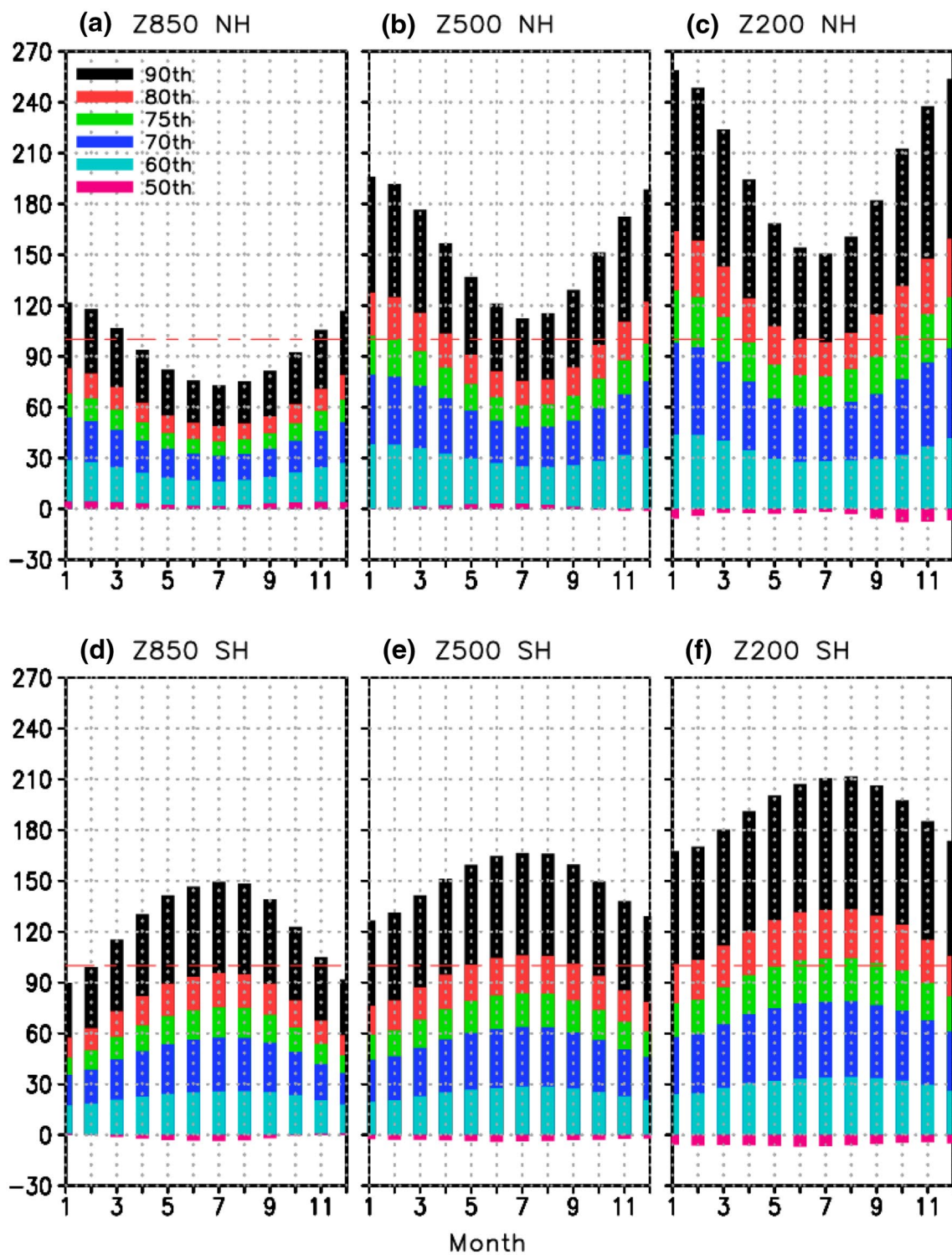
Fig. 10 Major percentiles of zonal eddy anomalies (GPM) for each month at Z850 (left), Z500 (middle) and Z200 (right) in the NH (up) and SH (bottom)

the mask. This maximum-searching procedure can absorb some subtropical grids into blocking (e.g., Fig. 1c2). However, it is better than searching a maximum in latitude or longitude order which may start from a subtropical high and include mid-latitude grids to be discarded by later tracking. In addition, each separated high system covers at least 15°

Fig. 11 BE occurrence frequencies at Z200 (**a**, **b**), Z500 (**c**, **d**), Z850 (**e**, **f**) in the NH during DJF (left column) and JJA (right column) seasons. Dots represent all mass-weighted centers of the blocking highs in each panel. The colored range is limited to 3–24% for a better comparison
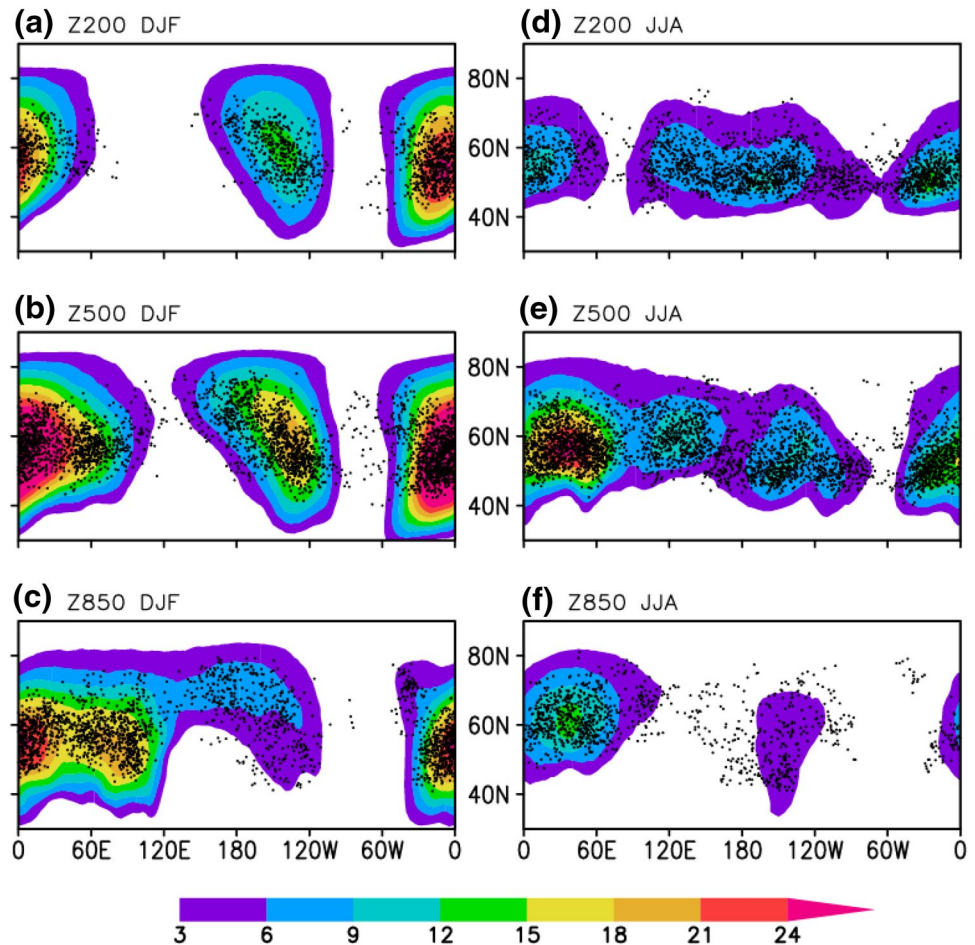
consecutive longitudes (to be shown in Sect. 6), meeting the large-scale requirements (e.g., Davini et al. 2012).

5.2 Identification of IBs

An IB requires a reversal of meridional gradients of Z on at least one grid at the latitude interval (40°, 80°) and inside the identified high. This requirement automatically excludes low-latitude blocks for consideration. In the NH, the GHGS is the gradient between the grid and 40° N and the GHGN is that between 80° N and the grid. Once the two conditions of TM1990 are met, i.e., GHGS > 0 and GHGN < − 10 GPM/° latitude on this grid, the high is determined as an IB. This way in determining the reversals is equivalent to examining any latitude as the CBL inside the high. The same procedure with sign changes determines an IB in the SH. The highs without any reversal are reset to 0 on the mask map. After all highs are examined, their corresponding numbers on the mask map are compacted to exclude non-blocking highs.

5.3 Tracking BEs

Quasi-stationary and persistent conditions are imposed to track each BE. The quasi-stationarity is determined by a distance of no more than 10° longitudes between the mass-weighted centers of two consecutive IBs with maximum overlap. In each IB, grids with Z^* greater than 75% of the maximum are scaled with their corresponding Z^* values for their mass-weighted center in longitude and latitude. The distance threshold means that the IB moves slower than ~ 10 m s^{-1}. This threshold is applied to all cases, because most BEs propagate much slower than the threshold (to be shown by the distributions of moving speeds in Sect. 6). The two criteria lead to reasonable results compared to a single requirement of at least 50% overlap between the IBs, as statistics (not shown) indicates that the latter leads to more BEs, close to lifting the distance threshold to 25° longitudes per day. In addition, grids with at least 75% Z^* of the maximum are reasonable to determine the IB center and propagating speeds, as too small and too large percentages sometimes result in very large distance to break the BE (not shown).
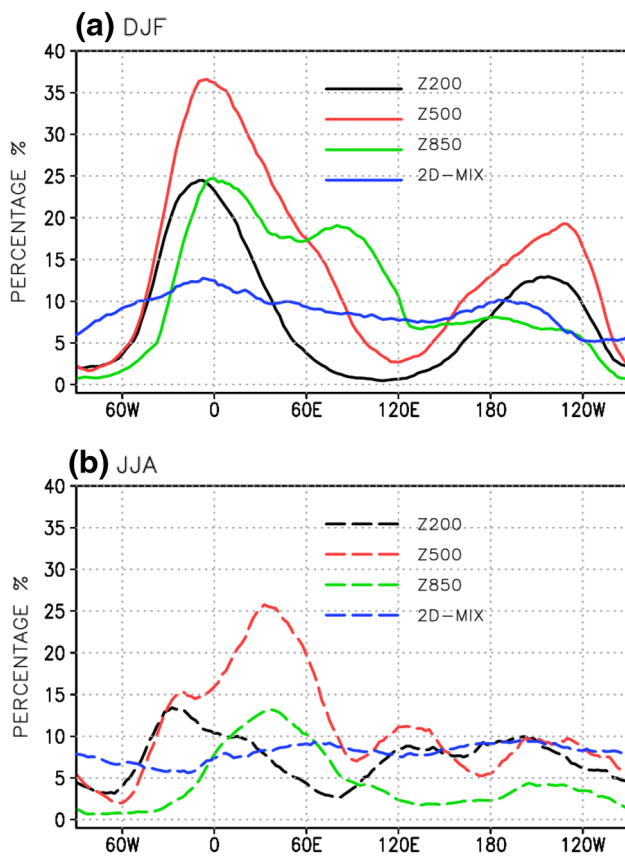
Fig. 12 BE maximum occurrence frequencies with longitude at Z200 (black), Z500 (red), and Z850 (green) in the NH during DJF (**a**) and JJA (**b**). The 2D-MIX for Z500 (blue) is also plotted for comparison

The persistence of BEs in days was defined slightly differently in existing blocking indices. A shorter-time threshold generally results in more BE occurrences. We choose 4 days in the new index as in the TM1990.

Two algorithms with different computing efficiency have tracked identical BEs in the data. The first finds a starting IB and tracks the rest. It is repeated on new IBs until the end of the data. This algorithm cannot determine whether a track should be kept near the end of the data when the persistence has not reached the 4-day threshold. It is thus less suitable for real-time applications. The second algorithm starts a track for each IB in the beginning of the data, and updates each track every day afterwards by adding a new segment satisfying the quasi-stationarity or finishing the track for a BE by the persistence criterion. An IB that cannot be added to any track starts a new one. This algorithm is computationally faster than the first and suitable for real-time detection by recording quasi-stationary IBs before reaching the 4-day threshold. The above processes have been applied to the Z fields at different vertical levels in the SH and NH during different seasons. Discussed next are BE climatologies in those situations.

6 Climatologies of Blocking Highs

IBs and BEs during past decades have been detected and tracked by the new index. Overall the climatologies of IBs have distributions similar to those of BEs but with larger values (not shown). BE climatologies are compared next, focusing on the similarities and differences at vertical levels in the NH and SH. Figure 11 shows 2-D distributions of BE occurrence frequencies (color shading) superimposed with mass-weighted centers (black dots) of blocking highs at Z200 (top), Z500 (middle) and Z850 (bottom) in the NH during DJF (left) and JJA (right), and Fig. 12 plots the maximum occurrence at each longitude in each case. Overall BEs manifest evident seasonality, geographical preference and quasi-barotropicity. Specifically during DJF, BEs at Z500 (Fig. 11b) occur primarily in the Atlantic-Europe with a maximum of 36% near 5° W and secondarily in the Northeastern Pacific with a maximum of 19% near 125° W (red in Fig. 12a). BEs at Z200 (Fig. 11a) also concentrate on the two sectors, with a maximum of 25% near 5° W and another of 13% near 150° W (black in Fig. 12a). BEs at Z850 (Fig. 11c) occur most frequently near 5° W as well, with a maximum of 20% and a secondary near 80° E of 18% (green in Fig. 12a). In contrast during JJA (Fig. 11e, f), BEs occur much less frequently. The maximum occurrence reduces to 25% and shifts to 30° E at Z500 (red in Fig. 12b), reduces to 13% and shifts to 30° W at Z200 (black in Fig. 12b), and reduces to 13% and shifts to 40° E at Z850. The substantial reductions in JJA indicate strong seasonality of BE occurrences.

The geographical preference is evident, as BEs occur in the Atlantic-Europe and Pacific sectors much more frequently than elsewhere at the three levels in the NH during DJF and JJA (Figs. 11, 12). In particular, the maximum occurrence near 5° W is about or more than double to that near 130–140° W (Fig. 12). The quasi-barotropicity is particularly evident in the Atlantic-Europe during DJF, as the maximum is located near 5° W at Z200, Z500 and Z850 (Fig. 11a–c). It is also evident at Z200 and Z500 in the Northeastern Pacific during DJF, while less evident at Z850 with dramatically smaller frequencies than above (Fig. 11a–c). The barotropicity in JJA is still evident at Z200 and Z500 in the eastern Atlantic and East Asia at about 120° E (Figs. 11d, e, 12b). It is noteworthy that the barotropicity in BEs appears less evident over Europe and western Pacific during JJA, as the occurrence centers are tilted westward with altitude (Fig. 11d–f). In addition, BEs occur most frequently at Z500 among the three vertical levels in both Atlantic-Europe and Pacific sectors during DJF and JJA. The dots in Fig. 11 concentrate mostly around the Atlantic-Europe and Pacific in DJF and JJA, indicating the geographical preference as well.
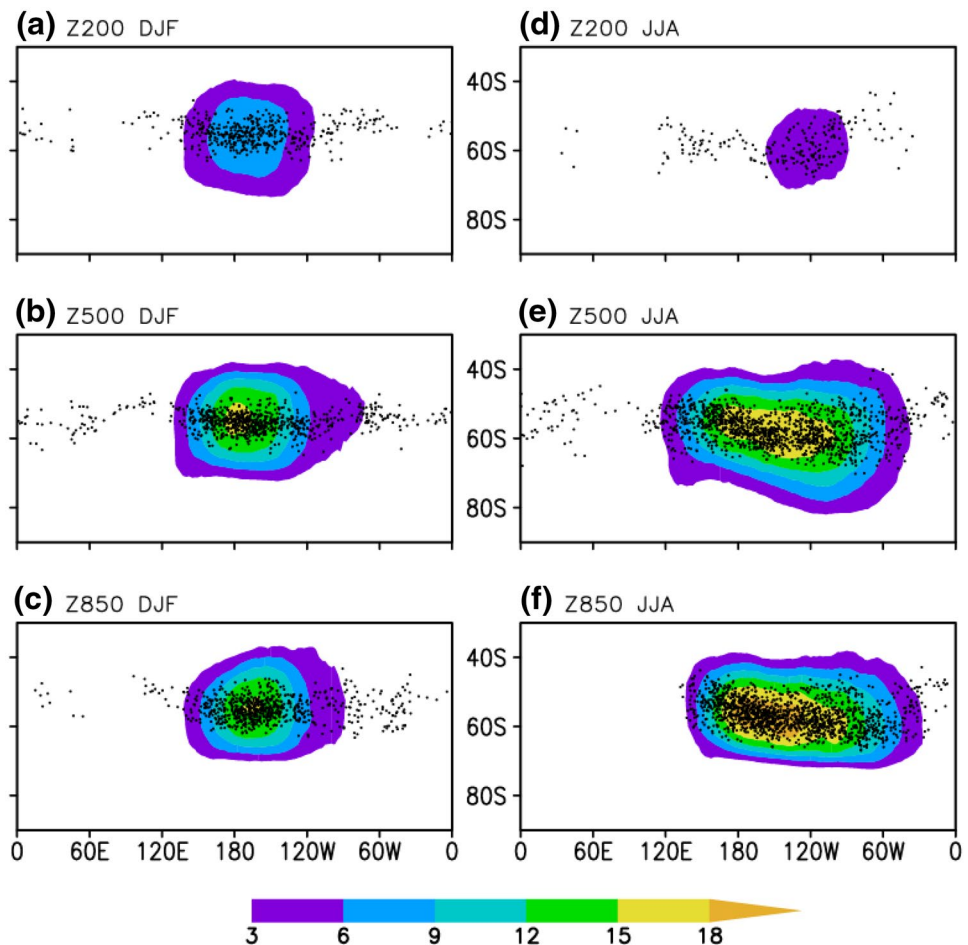
Fig. 13 Same as Fig. 11 but for the SH

Figure 12 also compares the 1-D maximum occurrence frequencies of BEs at Z500 detected by the 2-D MIX (Woollings et al. 2018; blue). In DJF (Fig. 12a), the Atlantic-Europe peak near 5° W is only 13% in the MIX, about 2/5 of that in the new Eddy-ABS (red). The Pacific peak near 170° W is 10% in the MIX, about half of that in the new index. The dramatically more occurrences in the new index are caused primarily by the CBLs at any latitude. However, at 120° E for (75° E–170° E) and 90° W for (100° W–50° W), the MIX detected about 7–8% BE occurrences while the Eddy-ABS detected about 3%. A composite of Z500 for the different events at each of the two longitudes indicate a similar pattern of positive time anomalies over climatological troughs (not shown); these are misidentifications. In JJA (Fig. 12b), the MIX identified less BE occurrences in 50° W–65° E and more in other longitudes. The causes are also misidentifications because blocking highs with zonal eddy anomalies above the 75th percentile are not required for the BEs in the MIX.

In the SH, BE climatologies also manifest evident seasonality, geographical preference and quasi-barotropicity but with notable differences. In DJF (Fig. 13a–c), the BE centers concentrate in 150° E–120° W and 65° S–55° S at Z200,

Z500 and Z850, with a maximum occurrence at 175° W and about 15% at Z500 and Z850, and 8% at Z200 (Fig. 14a). This alignment indicates evident barotropicity. In JJA (Fig. 13d–f), BEs concentrate in the Southern Pacific while the centers spread more than those in DJF. Correspondingly the maximum occurrence is 15–12% from 175° E–90° W at Z500 (red in Fig. 14b) and Z850 (green), and 4% from 150° W–95° W at Z200 (black in Fig. 14b), indicating evident quasi-barotropicity and geographical preference. The notably lower occurrences at Z200 in JJA than DJF indicate strong seasonality.

Properties of BEs, including the lifetime, maximum intensity, minimum width, average area and moving speed, show comparable distributions at Z200, Z500 and Z850 in the NH and SH during DJF and JJA. The lifetime of BEs detected by previous 1-D or 2-D blocking indices is known to have a log-linear distribution (e.g., Pelly and Hoskins 2003). This distribution is also robust in the many more BEs at Z500 and the BEs at Z200 and Z850 in both hemispheres detected by the Eddy-ABS approach (not shown). Figure 15 shows the histograms and best-fitted distributions for other properties of all BEs at Z500. The maximum intensity of BEs, represented by the maximum Z^* of a member blocking
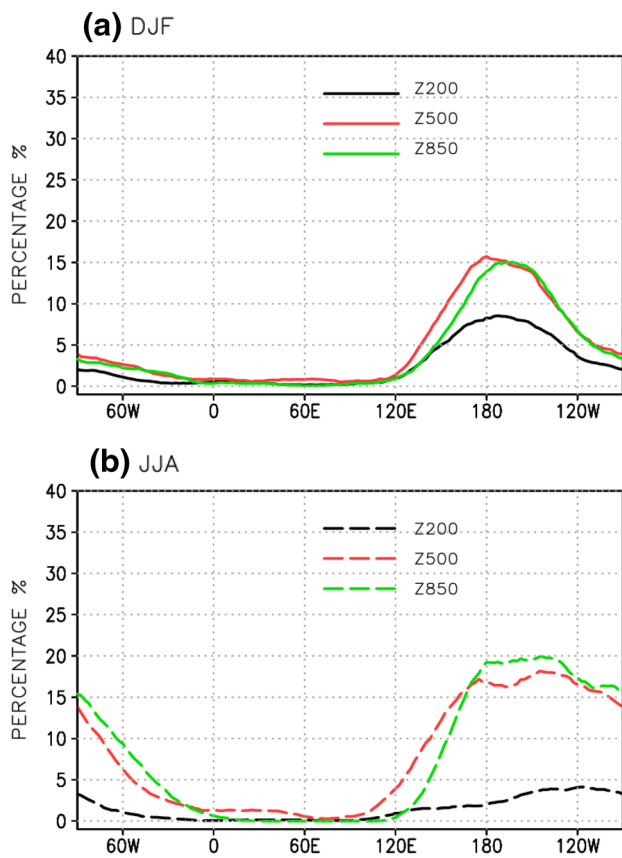
(a) DJF

(b) JJA

Fig. 14 Same as Fig. 12 but for the SH

high, has a log-normal distribution in the NH (Fig. 15a) but a normal distribution in the SH (Fig. 15b). The minimum width, represented by the smallest difference in longitudes between the western and eastern boundaries, has a log-normal distribution in both hemispheres (Fig. 15c, d). It is noteworthy that nearly all BEs have a minimum width larger than 20° longitudes, satisfying the large-scale requirement of blocking with at least 15° (e.g., Davini et al. 2012; Woollings et al. 2018). The average area of all member blocking highs has a log-normal distribution in both hemispheres (Fig. 15e, f). The areas are generally smaller than 2×10^6 km^2, a threshold in the ANO and MIX indices in Woollings et al. (2018). This is because positive Z^* correspond only to a ridge or high on Z, not a weakened trough. Finally the moving speed has a normal distribution in both hemispheres (Fig. 15g, h). The average speed is mostly about 4°–5° longitudes per day and barely reaches 10°, indicating the 10° is a reasonable threshold for the quasi-stationarity. These distributions are correspondingly the same at Z200 and Z850 (not shown).

The maximum intensity of BEs is a property worth more discussion, as in Davini et al. (2012). There is a strong linear dependence between the maximum intensity and lifetime of BEs at Z500, as shown by their scatter plots superimposed with a linear regression line (Fig. 16). Since the log-linear distribution for the lifetime is different from the log-normal for the maximum intensity in the NH, the regression corresponds to a correlation coefficient of 0.25 for a total of 2574 BEs, which is still well above the 99% significance level. The coefficient is 0.29 for the 919 BEs at Z500 in the SH. This indicates that stronger blocking highs tend to persist longer in time.

Table 1 summarizes the linear correlations of the maximum intensity with other properties at Z200, Z500 and Z850 in the NH and SH. The number of BEs is 2574 at Z500 in the NH, the largest among all cases, and only 290 at Z200 in the SH, the smallest. With those many BEs, the moving speeds do not show any linear dependence on the maximum intensity, as the correlation is nearly 0. All other properties in Table 1 show a significant linear correlation with the maximum intensity, however, as even the smallest correlation of 0.18 for the Z200 in the NH is above the 99% significance level. These strong correlations indicate that the maximum intensity is a good proxy of a BE.

7 Summary and discussions

Detailed comparisons indicate that several typical blocking indices in 1-D and 2-D have detected contrasting climatologies of past BEs. The differences are largely caused by misses or misidentifications. Two factors are fundamentally responsible: (1) the CBLs are specified, and (2) large positive time anomalies of geopotential height deviate away from blocking highs. Based on the comparison, a new 2-D Eddy-ABS index is developed to identify all types of blocks targeting their high-pressure components. The index selects closed zonal eddy anomalies Z^* at 850, 500 and 200 hPa above the 75th percentile of each month as candidates. It seeks a reversal of meridional gradients of Z at 40°–80° inside a high candidate, which is equivalent to the CBL at any latitude. It adopts three thresholds for the reversals of height gradients (i.e., GHGS > 0 and GHGN < − 10 GPM/°) for IBs, moving speeds of 10° longitudes per day with maximum overlap for quasi-stationarity and at least 4 days persistence for BEs. These conditions make the index a unified type to identify blocks at three vertical levels in both NH and SH during different seasons. The definition and thresholds of blocking highs reasonably avoid cut-off low structures and marginal ridges at Z500, which were misidentified by the 2-D ABS, ANO or MIX indices (Woollings et al. 2018).
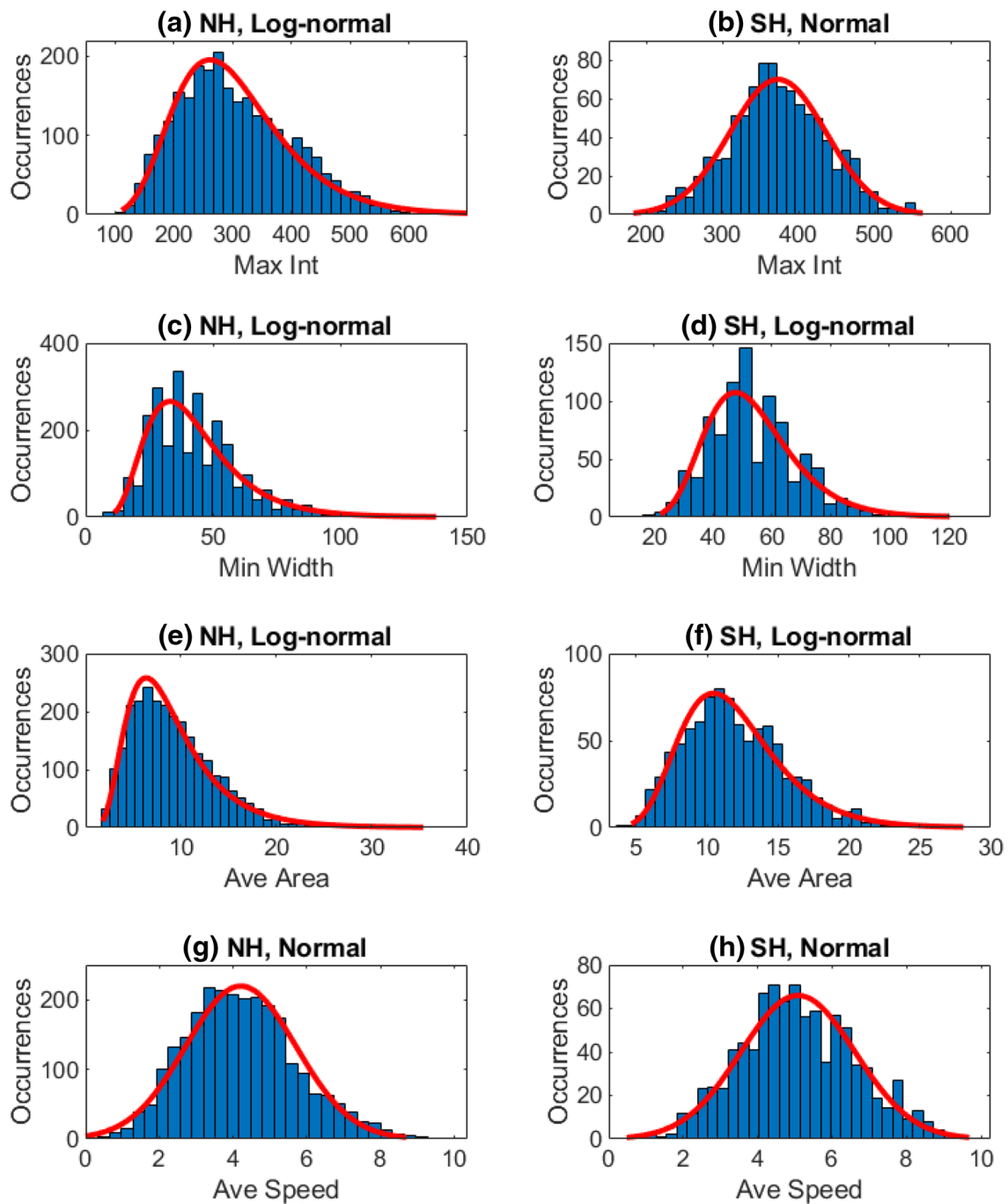
Fig. 15 Histograms and best-fitted distributions of all tracked BE highs at Z500 for the maximum intensity (GPM; **a**, **b**), minimum width (degree longitudes; **c**, **d**), average area (10^5 km²; **e**, **f**) and aver- aged moving speed (degree longitudes per day; **g**, **h**) in the NH (left column) and SH (right column)

The new index has identified many more IBs and BEs at Z500 in the NH than the several indices did, because the varying CBLs represent the day-to-day variations of jet streams and blocking better than those fixed on each longitude. The detected BEs retain evident geographical preference and seasonality in the NH, contrasting other 2-D indices in notably

Fig. 16 Linear dependency of the lifetime on the maximum intensity for all BEs at Z500 in the NH (**a**) and SH (**b**)
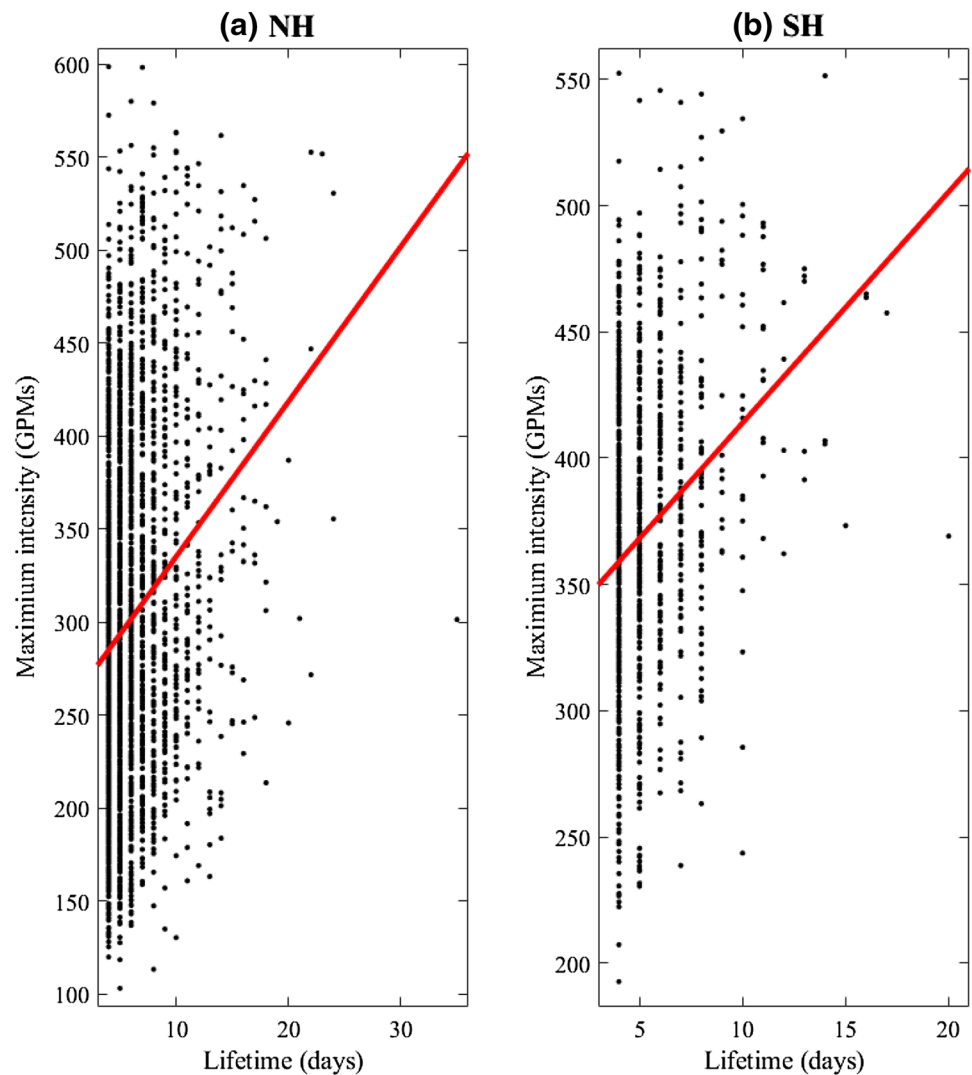

Table 1 Linear correlations between the maximum intensity and lifetime, average width, minimum width, average area covered, minimum area and average speed of all BEs at Z200, Z500 and Z850 in the NH and SH detected by the new Eddy-ABS index

Hemisphere	Vertical levels	Total events	Lifetime	Average width	Minimum width	Average area	Minimum area	Average speed
NH	Z200	1667	0.18	0.65	0.60	0.77	0.68	−0.06
	Z500	2574	0.25	0.64	0.52	0.79	0.62	−0.04
	Z850	1300	0.35	0.49	0.38	0.67	0.50	−0.06
SH	Z200	290	0.24	0.54	0.50	0.68	0.61	−0.06
	Z500	919	0.29	0.49	0.37	0.67	0.48	−0.05
	Z850	969	0.32	0.54	0.44	0.64	0.48	−0.04

deteriorating these features. The BEs have a quasi-barotropic structure at Z850, Z500 and Z200, although the barotropicity changes with location and season and becomes less evident over Europe in JJA. These BE features are also disclosed in the SH for the first time. Several properties of tracked BE highs in both hemispheres, including the maximum

intensity, lifetime, average width in longitudes and average area, have different statistical features: the lifetime has a log-linear distribution, the average area has a log-normal distribution and the moving speed has a normal distribution. The maximum intensity is strongly correlated with other properties except the moving speed. Among the correlations, the lifetime has the lowest value because of the different distributions. It is noteworthy that the maximum intensity has a log-normal distribution in the NH, different from the normal distribution in the SH. The log-normal distribution was found to occur in the finite-amplitude local Rossby wave activity (Nakamura and Huang 2018; their Fig. 5 in S1) in the NH during DJF season. Whether a dynamical relationship connects the Rossby wave activities with BE properties merits more analysis.

In addition to the similarities, the BE climatologies are notably different in the vertical. In the NH, Z500 has the most BE occurrences, Z200 has less and Z850 the least, particularly over the Atlantic-Europe and Northeast Pacific during DJF. In the SH, Z500 also has the most BE occurrences, while Z850 has slightly less and Z200 has the least, particularly during JJA. These differences suggest that the BE lifetime from onset to decay might be associated with different dynamical processes in the vertical direction.

There are other notable hemispheric differences in BE climatologies as well. In particular BEs occur as a dipole pattern in the Atlantic-Europe and Pacific in the NH, while as a monopole pattern near the date line in the SH. The quasi-barotropicity is more evident in the middle-upper troposphere in the NH, while more evident in the lower-middle troposphere in the SH. In addition, the maximum intensity of BEs is much larger in the NH. Whether and how these differences are associated with different dynamics, land-sea contrast and mountain distributions in the two hemispheres merit more investigation. In summary, the new Eddy-ABS index provides a unified approach for tracking blocking highs in globally gridded data sets.

Appendix

See Table 2.

Table 2 Brief comparison of several blocking indices mentioned in the text

Index	Dimension	CBL	ABS reversal	Z' Time anomaly	Stationarity	Persistence (days)
TM1990	Longitude	60° N	GHGS > 0 and GHGN < −10			4
PH2003 (1D-ABS)	Longitude	Max EKE300	GHGS > 0 and GHGN < −10			4
Scherrer2006	Longitude–latitude	Any in 35−75° N	GHGS > 0 and GHGN < −10			5
Davini2012 (2D-ABS)	Longitude–latitude	Any in 35−75° N	Also GHGS2 < −5		> 15° longitude	5
DG1983 (ANO)	Longitude–latitude			> 90th perc. > 2×10^6 km^2	> 50% overlap	5
Barriopedro-2010	Longitude–latitude	Max var. of Z500	15°-lat ave reversal	> 1 STD, after ABS	> 50% overlap	4
Dunn-Sigouin2013	Longitude–latitude	Max anomaly	Negative to the south	> 1.5 STD before ABS	> 50% overlap	5
Woollings2018(MIX)	Longitude–latitude	Max var. of Z500	Negative to the south	> 90th perc. before ABS	> 50% overlap	5

References

Barriopedro D, Garcia-Herrera R, Lupo AR, Hernandez E (2006) A climatology of Northern Hemisphere blocking. J Clim 19:1042–1063

Barriopedro D, Garcia-Herrera R, Gonzalez-Rouco JF, Trigo RM (2010) Application of blocking diagnosis methods to general circulation models. Part I: a novel detection. Clim Dyn 35:1373–1391

Brunner L, Hegerl GC, Steiner AK (2017) Connecting atmospheric blocking to European temperature extremes in spring. J Clim 30:585–594

Carrera ML, Higgins RW, Kousky VE (2004) Downstream weather impacts associated with atmospheric blocking over Northeast Pacific. J Clim 17:4823–4839

Colucci SJ, Kelleher ME (2015) Diagnostic comparison of tropospheric blocking events with and without sudden stratospheric warming. J Atmos Sci 72:2227–2240

D'Andrea F, Tibaldi S, Blackburn M, Boer G, Déqué M, Dix MR, Dugas B, Ferranti L, Iwasaki T, Kitoh A, Pope V, Randall D, Roeckner E, Straus D, Stern W, Van den Dool H, Williamson D (1998) Northern Hemisphere atmospheric blocking as simulated by 15 atmospheric general circulation models in the period 1979–1988. Clim Dyn 14:385–407

Davini P, Cagnazzo C, Gualdi S, Navarra A (2012) Bidimensional diagnostics, variability, and trends of Northern Hemisphere blocking. J Clim 25:6496–6509

Davini P, Cagnazzo C, Fogli PG, Manzini E, Gualdi S, Navarra A (2014) European blocking and Atlantic jet stream variability in the NCEP/NCAR reanalysis and the CMCC-CMS climate model. Clim Dyn 43:71–85

Diao Y, Li J, Luo D (2006) A new blocking index and its application: blocking action in the Northern Hemisphere. J Clim 19:4819–4839

Doblas-Reyes FJ, Casado MJ, Pastor MA (2002) Sensitivity of the Northern Hemisphere blocking frequency to the detection index. J Geophys Res 107(D2):4009. https://doi.org/10.1029/2000JD000290

Dole RM (1986) Persistent anomalies of the extratropical Northern Hemisphere wintertime circulations: structure. Mon Weather Rev 114:178–207

Dole RM, Gordon ND (1983) Persistent anomalies of the extratropical Northern Hemisphere wintertime circulation: geographical distribution and regional persistence characteristics. Mon Weather Rev 111:1567–1586

Dunn-Sigouin E, Son SW, Lin H (2013) Evaluation of Northern Hemisphere blocking climatology in the Global Environment Multiscale (GEM) model. Mon Weather Rev 141:707–727

Kalnay E, Kanamitsu M, Kistler R, Collins W, Deaven D, Gandin L, Iredell M, Saha S, White G, Woollen J, Zhu Y, Chelliah M, Ebisuzaki W, Higgins W, Janowiak J, Mo K, Ropelewski C, Leetmaa A, Reynolds R, Jenne R (1996) The NCEP/NCAR 40-year reanalysis project. Bull Am Meteorol Soc 77:437–471

Lejenäs H, Økland H (1983) Characteristics of northern hemisphere blocking as determined from long time series of observational data. Tellus 35A:350–362

Liu P, Zhu Y, Zhang Q, Gottschalck J, Zhang M, Melhauser C, Li W, Guan H, Zhou X, Hou D, Pena M, Wu G, Liu Y, Zhou L, He B, Hu W, Sukhdeo R (2018) Climatology of tracked persistent maxima of 500-hPa geopotential height. Clim Dyn 51:701–717

Nakamura N, Huang CSY (2018) Atmospheric blocking as a traffic jam in the jet stream. Scinece 361(6397):42–47. https://doi.org/10.1126/science.aat0721

Park YJ, Ahn JB (2014) Characteristics of atmospheric circulation over East Asia associated with summer blocking. J Geophys Res Atmos 119:726–738

Pelly JL, Hoskins BJ (2003) A new perspective on blocking. J Atmos Sci 60:743–755. https://doi.org/10.1175/1520-0469(2003)060,0743:ANPOB.2.0.CO;2

Pfahl S, Wernli H (2012) Quantifying the relevance of atmospheric blocking for co-located temperature extremes in the Northern Hemisphere on (sub-)daily time scales. Geophy Res Lett 39:L12807

Renwick JA (2005) Persistent positive anomalies in the Southern Hemisphere circulation. Mon Weather Rev 133:977–988

Rex DF (1950) Blocking action in the middle troposphere and its effect upon regional climate. II. The climatology of blocking action. Tellus 2:275–301

Rodrigues RR, Woollings T (2017) Impact of atmospheric blocking on South America in Austral summer. J Clim 30:1821–1837

Sausen R, Konig W, Sielmann F (1995) Analysis of blocking events observation and ECHAM model simulations. Tellus 47A:421–438

Scherrer SC, Croci-Maspoli M, Schwierz C, Appenzeller C (2006) Two-dimensional indices of atmospheric blocking and their statistical relationship with winter climate patterns in the Euro-Atlantic region. Int J Climatol 26:233–249

Schwierz C, Croci-Maspoli M, Davies HC (2004) Perspicacious indicators of atmospheric blocking. Geophys Res Lett 31:L06125. https://doi.org/10.1029/2003GL019341

Sousa P, Trigo RM, Barriopedro D, Soares PMM, Ramos AM, Liberato MLR (2017) Responses of European precipitation distributions and regimes to different blocking locations. Clim Dyn 48:1141–1160

Tibaldi S, Molteni F (1990) On the operational predictability of blocking. Tellus 42:343–365

Woollings T, Barriopedro D, Methven J, Son SW, Martius O, Harvey B, Sillmann J, Lupo AR, Seneviratne S (2018) Blocking and its response to climate change. Curr Clim Change Rep 4:287–300

Yamada TJ, Takeuchi D, Farukh MA, Kitano Y (2016) Climatological characteristics of heavy rainfall in Northern Pakistan and atmospheric blocking over Western Russia. J Clim 29:7743–7754